Self-critical machine-learning wall-modeled LES for external aerodynamics

By A. Lozano-Durán AND H. J. Bae†

1. Motivation and objectives

The use of computational fluid dynamics (CFD) for external aerodynamic applications has been a key tool for aircraft design in the modern aerospace industry. However, flow predictions from the state-of-the-art solvers are still unable to comply with the stringent accuracy requirements and computational efficiency demanded by the industry. In recent years, wall-modeled large-eddy simulation (WMLES) has gained momentum as a high-fidelity tool for routine industrial design. In WMLES, only the large-scale motions in the outer region of the boundary layer are resolved, which enables a competitive computational cost compared with other CFD approaches (Choi & Moin 2012). As such, NASA has recognized WMLES as an important pacing item for "developing a visionary CFD capability required by the notional year 2030" (Slotnick *et al.* 2014). In the present brief, we introduce a wall model based on the flow-state classification that is also self-critical, i.e., it provides a confidence value for the classification.

Several strategies for modeling the near-wall region have been explored in the literature, and comprehensive reviews can be found in Cabot & Moin (2000), Piomelli & Balaras (2002), Spalart (2009), Larsson *et al.* (2016), and Bose & Park (2018). One of the most widely used approaches for wall modeling is the wall-flux modeling approach (or approximate boundary conditions modeling), where the no-slip and thermal wall boundary conditions are replaced with stress and heat-flux boundary conditions provided by the wall model. This category of wall models utilizes the large-eddy simulation (LES) solution at a given location in the LES domain as input and returns the wall fluxes needed by the LES solver. Examples of the most popular and well-known approaches are those computing the wall stress using either the law of the wall (Deardorff 1970; Schumann 1975; Piomelli *et al.* 1989), the full/simplified RANS equations (Balaras *et al.* 1996; Wang & Moin 2002; Chung & Pullin 2009; Bodart & Larsson 2011; Kawai & Larsson 2013; Bermejo-Moreno *et al.* 2014; Park & Moin 2014; Yang *et al.* 2015) or dynamic wall models (Bose & Moin 2014; Bae *et al.* 2019).

In recent years, advances in machine learning and data science have incited new efforts to complement the existing turbulence modeling approaches in the fluids community. However, machine learning is still far from being the panacea to solve long-standing problems in LES. The statement "LES modeling will be solved by machine learning" is as meaningful as "LES modeling will be solved by the Fourier transform", i.e., not very. Machine learning is a tool, as much as the Fourier transform is a tool. Both might aid the modeling of turbulent flows if properly used. Ultimately, in-depth knowledge of the physics to be modeled and the formulation of the problem in a language consistent with machine learning is key to utilizing the tool to its fullest potential.

Supervised learning, i.e., the machine-learning task of learning a function that maps an input to an output based on provided training input-output pairs, was first introduced in turbulence modeling in the form of subgrid-scale (SGS) modeling for LES.

† Harvard University

Early approaches used neural networks to emulate and speed up a conventional, but computationally expensive, SGS model (Sarghini *et al.* 2003). More recently, SGS models have been trained to predict the (so-called) perfect SGS terms using data from filtered direct numerical simulation (DNS) (Gamahara & Hattori 2017; Xie *et al.* 2019). Other approaches include deriving SGS terms from optimal estimator theory (Vollant *et al.* 2017) and deconvolution operators (Hickel *et al.* 2004; Maulik & San 2017; Fukami *et al.* 2019). One of the first attempts at using supervised learning for WMLES can be found in Yang *et al.* (2019). These authors noted that a model trained on channel flow data at a single Reynolds number could be extrapolated to higher Reynolds numbers and similar configurations. The model relied on information about the flow that is typically inaccessible in real-world applications, such as the boundary-layer thickness, and was limited to channel flow configurations. The reader is referred to Duraisamy *et al.* (2019) and Brunton *et al.* (2020) for a literature review on machine learning for fluid mechanics.

Currently, the major challenge for WMLES of realistic external aerodynamic applications is achieving the robustness and accuracy necessary to model the myriad of different flow regimes that are characteristic of these problems. Examples include turbulence with mean-flow three-dimensionality, laminar-to-turbulent transition, flow separation, secondary flow motions at corners, and shock wave formation, to name a few. The wall-stress generation mechanisms in these complex scenarios differ from those in flat plate turbulence. However, the most widespread wall models are built upon the assumption of statistically-in-equilibrium wall-bounded turbulence, which only applies to a handful number of flows. The latter raises the question of how to devise models capable of seamlessly accounting for such a vast and rich collection of flow physics in a single unified approach.

In the present brief, we develop a wall-flux-based wall model for LES using a self-critical machine-learning approach. Since data-driven models are limited by the information they are provided, the model is formulated to naturally account for various flow configurations. In this preliminary work, the wall model is trained on DNS data of flow over a flat plate, flow in a turbulent duct, and separated flow at various Reynolds numbers. The model comprises two components: a classifier and a predictor. The classifier is trained to place the flows into the separate categories along with a confidence value, while the predictor outputs the modeled wall stress based on the likelihood of each category. The model is validated on a flow over the fuselage and wing-body junction of the NASA Juncture Flow Experiment.

This brief is organized as follows. The flow setup, mathematical modeling, and numerical approach are presented in Section 2. Results for WMLES with a widely used equilibrium wall model are presented in Section 3. The results include the prediction of the mean velocity profiles for three different locations on the aircraft: the upstream region of the fuselage, the wing-body juncture, and wing-body juncture close to the trailing edge. The formulation of the new model is discussed in Section 4. The model is validated in Section 5 and compared with the equilibrium wall model. Finally, conclusions are offered in Section 6.

2. Simulation setup and methods

2.1. *NASA Juncture Flow*

The problem considered is the NASA Juncture Flow, which has been recently proposed as a validation experiment for generic wing-fuselage junctions at subsonic conditions (Rumsey *et al.* 2019). The experiment consists of a full-span wing-fuselage body configured

FIGURE 1. Experimental setup of the NASA Juncture Flow at NASA Langley 14- by 22-foot Subsonic Wind Tunnel.

with truncated DLR-F6 wings and has been tested in the Langley 14- by 22-foot Subsonic Tunnel (Figure 1). The Reynolds number is $Re = LU_\infty/\nu = 2.4$ million, where L is the chord at the Yehudi break, U_∞ is the freestream velocity and ν is the kinematic viscosity. The density of the air is ρ. We consider an angle of attack of $AoA = 5$ degrees. The experimental dataset comprises a collection of local-in-space time-averaged measurements (Kegerise *et al.* 2019), such as velocity profiles and Reynolds stresses, which greatly aid the validation of models and their ability to capture the critical flow physics. The frame of reference is such that the fuselage nose is located at $x = 0$, the x-axis is aligned with the fuselage centerline, the y-axis denotes the spanwise direction, and the z-axis is the vertical direction. The associated instantaneous velocities are denoted by u, v, and w, and occasionally by u_1, u_2, and u_3. Time-averaged quantities are denoted by $\langle\cdot\rangle$.

2.2. *Numerical methods and models*

We perform WMLES of the NASA Juncture Flow using the high-fidelity solver charLES. The reader is referred to Lozano-Durán *et al.* (2020) for a detailed description of the numerical methods, grid generation and modeling approach. Here, we provide an abridged description of the numerical setup. The code integrates the compressible LES equations using a kinetic-energy conserving, second-order accurate, finite volume method. The SGS model is the dynamic Smagorinsky model (Germano *et al.* 1991) with the modification by Lilly (1992). We utilize a wall model to overcome the restrictive grid-resolution requirements to resolve the small-scale flow motions in the vicinity of the walls. The working principle of WMLES is illustrated in Figure 2. Flow information from the LES grid at a wall-normal distance h is used as input to the wall model. The wall model predicts the wall stress τ_w and heat flux at the wall q_w, which are imposed back to LES as boundary conditions. We use an algebraic equilibrium wall model (EQWM) derived from the integration along the wall-normal direction of an assumed constant-stress layer (Wang & Moin 2002; Kawai & Larsson 2012; Larsson *et al.* 2016). At each point of the wall $\boldsymbol{x}$, this yields an equation for the wall-model mean velocity profile

$$u_{||}^+(y_n^+) = \begin{cases} y_n^+ + a_1(y_n^+)^2 & \text{for } y_n^+ < y_n^{\text{ref}}, \\ \frac{1}{\kappa}\ln(y_n^+) + B & \text{otherwise}, \end{cases} \tag{2.1}$$

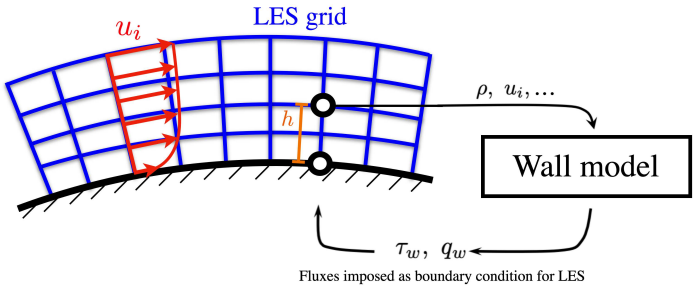

FIGURE 2. Schematic of the working principle of wall-modeled large-eddy simulation.

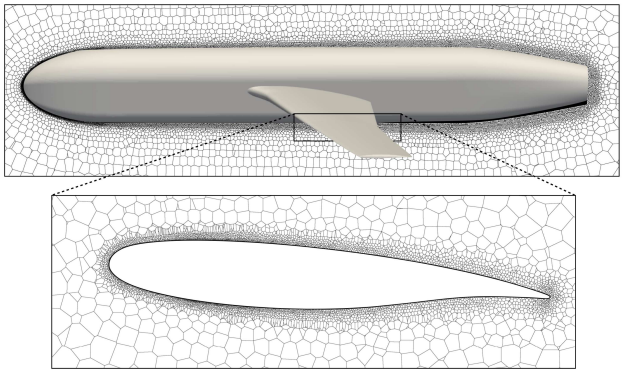

FIGURE 3. Visualization of Voronoi control volumes for boundary-layer-conforming grid with $N_{bl} = 5$ and $Re_\Delta^{\min} = 8 \times 10^3$ (see Lozano-Durán *et al.* 2020, for details).

where $u_{||}$ is the magnitude of the wall-parallel velocity, y_n is the wall-normal coordinate such that $y_n = 0$ is the wall, $+$ denotes normalization by ν and τ_w, $\kappa = 0.41$, $B = 5.2$, $y_n^{\text{ref}} = 23$, and $a_1 \approx -0.02$. The wall stress τ_w is computed by solving Eq. (2.1) iteratively evaluated at the wall-parallel LES velocity $u_{||}(\boldsymbol{x} + \boldsymbol{e}_2 h)$, where $\boldsymbol{e}_2$ is the wall-normal direction. The matching location h for the wall model is the first off-wall cell center of the LES grid. The walls are assumed isothermal. The modeling parameters in Eq. (2.1) are calibrated to match the wall-stress prediction for a zero-pressure-gradient turbulent boundary layer (ZPGTBL).

2.3. *Grid generation*

The mesh generation is based on the Voronoi tessellation of a collection of points. The points are seeded using a boundary-layer-conforming strategy such that the number of points per boundary-layer thickness is constant and equal to $N_{bl} = 5$. The minimum grid Reynolds number resolved is $Re_\Delta^{\min} \equiv \Delta_{\min} U_\infty / \nu = 8 \times 10^3$, where $\Delta_{\min}$ is the smallest grid size allowed. Figure 3 shows two cuts of the grid along the fuselage and wing, and Figure 4 contains an isosurface of the instantaneous Q-criterion.

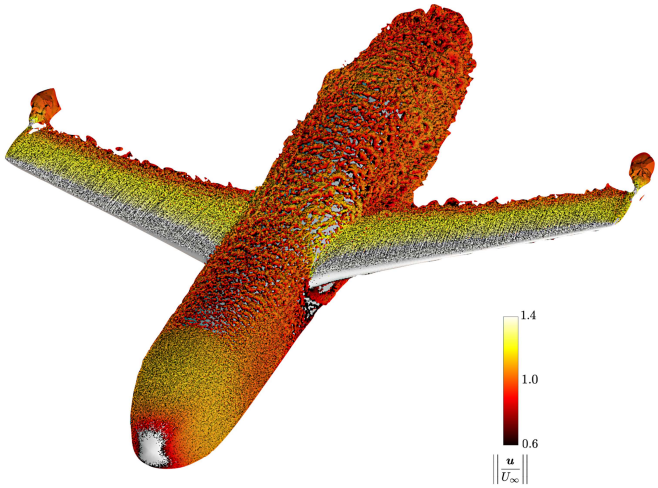

FIGURE 4. Visualization of the instantaneous isosurfaces of the Q-criterion colored by the velocity magnitude.

3. Results of WMLES with EQWM

The WMLES discussed above constitutes our baseline case. For reference, this case corresponds to case C-N5-Rem8e3 in Lozano-Durán *et al.* (2020). The prediction of the mean velocity profiles is shown in Figure 5 and compared with experimental measurements ($\boldsymbol{u}^{\text{exp}}$). Three locations are considered: the upstream region of the fuselage, the wing-body juncture†, and the wing-body juncture close to the trailing edge.

In the first region, the flow resembles a ZPGTBL. Hence, the dynamic Smagorinsky SGS model and the equilibrium wall-model in Eq. (2.1) perform accordingly (i.e., errors below 2%), as these have been devised for and validated in ZPGTBL. On the contrary, there is a decline of accuracy in the WMLES results in the wing-body juncture and trailing-edge region, which are dominated by secondary motions in the corner and flow separation. Lozano-Durán *et al.* (2020) have further shown that not only are the errors larger in the wing-body juncture and trailing-edge region, but the rate of convergence of WMLES by merely refining the grid is too slow to compensate for the modeling deficiencies.

The results above suggest that novel modeling venues must be exploited to improve WMLES predictions at an affordable computational cost. Here, we focus our efforts on wall model improvements. Nonetheless, we remark that physical insights, novel SGS modeling, and numerical/gridding advancements are also essential to attain robust high-accuracy WMLES. Future work will be devoted to devising an integrated modeling approach.

4. Model formulation

The working principle of the proposed model is summarized in Figure 6. The self-critical model (SCM) is comprised of two elements: a classifier and a predictor. First, the

† Note that this location differs from the wing-body juncture location selected in Lozano–Durán *et al.* (2020). The current location was chosen to highlight the deficiencies of the EQWM.

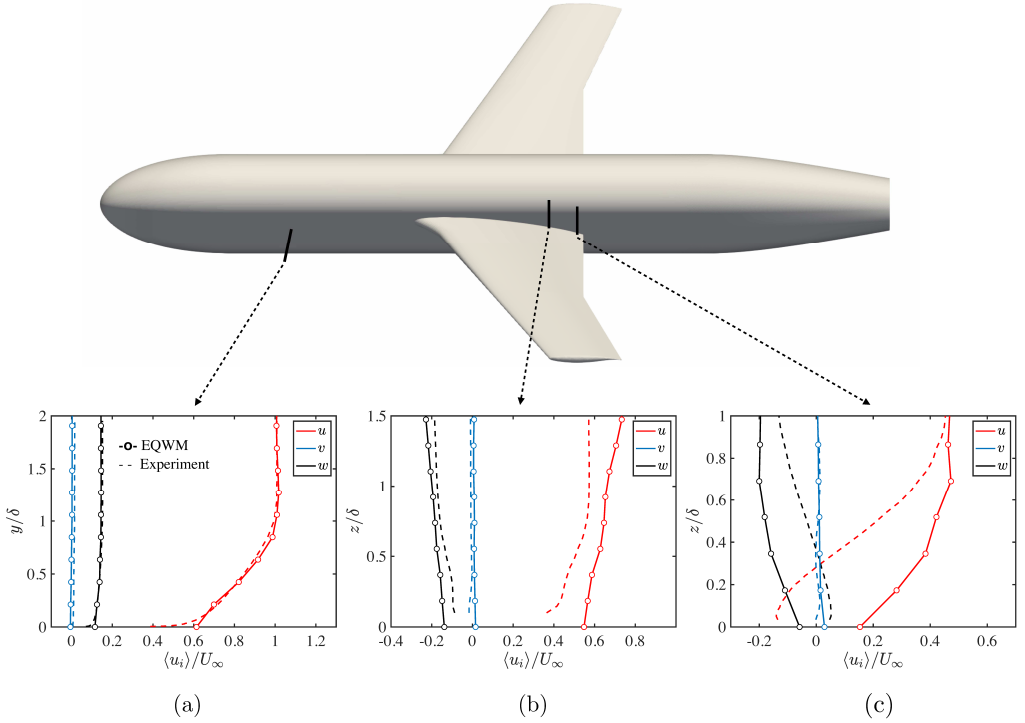

FIGURE 5. The mean velocity profiles at (a) upstream region of the fuselage at $x = 1168.4$ mm and $z = 0$ mm, (b) wing-body juncture at $x = 2747.6$ mm and $y = 239.1$ mm, and (c) wing-body juncture close to the trailing edge at $x = 2922.6$ mm and $y = 239.1$ mm. Solid lines with symbols denote WMLES with EQWM and dashed lines are experiments. Colors denote different velocity components. The distances y and z are normalized by the local boundary-layer thickness δ at each location.

classifier is fed with data from the LES solver and quantifies the similarities of the input with a collection of known building-block flows. The predictor leverages the information of the classifier to generate a wall-stress prediction via non-linear interpolation of the building-block database. The model is self-critical, i.e., it also outputs a high confidence value to the prediction if the input flow is recognized as a combination of the building blocks. If the input data looks extraneous, the model provides a low confidence value, which essentially means that the flow is unknown. We refer to the current version of the model as the SCM version 1 (SCMv1).

4.1. *Model requirements and assumptions*

We consider three basic model requirements. First, to comply with dimensional consistency, the inputs and outputs of the model should be given in non-dimensional form. Second, the model should be invariant under constant space/time translations and rotations of the frame of reference. Finally, the model should satisfy Galilean invariance, i.e., invariant under uniform velocity transformations of the frame of reference (Galilean invariance) or unidirectional accelerations in the case of incompressible flows (extended Galilean invariance).

The main model assumption is that the myriad of flow configurations encountered in external aerodynamics might be represented by a finite (hopefully small) set of canonical

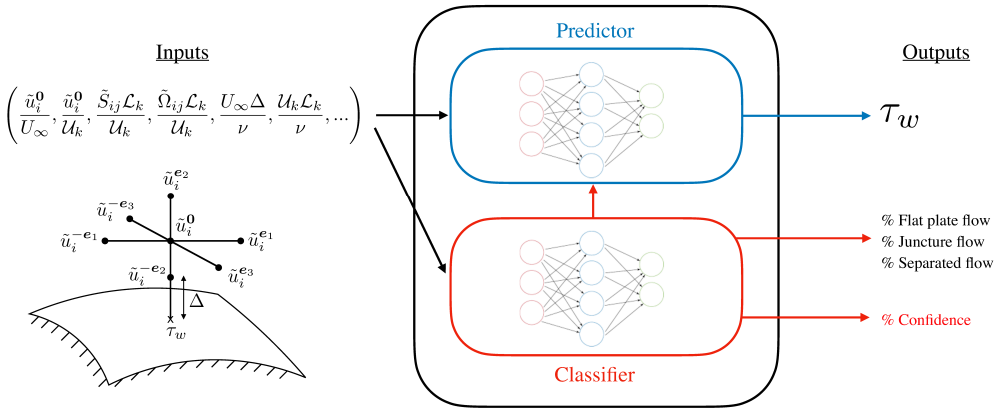

FIGURE 6. Schematic of the self-critical model (SCM). Details are provided in Section 4.2.

flow units. The assumption relies on the idea that a collection of building blocks contains the essential flow physics necessary to formulate generalizable models. In this preliminary work, the set of canonical units selected includes: turbulent channel flows, turbulent ducts, and turbulent boundary layers with separation. The three flow units are representative of ZPGTBL, turbulent flow in junctures, and separated turbulence, respectively. Examples of the three building-block units are included in Figure 7. The use of merely three building blocks is far from being representative of the rich flow physics (i.e., laminar flows, shock waves, compressibility effects, flow unsteadiness, adverse/favorable pressure gradients, other mean-flow three-dimensionalities and separation patterns, chemical reactions, etc.). Here, we test the model trained with only three building blocks and the collection will be extended in upcoming versions.

4.2. *Input and output variables*

The input velocity is acquired using a seven-point stencil as shown in Figure 6. The center of the stencil, $\boldsymbol{x}^{\boldsymbol{0}}$ is located at a wall-normal distance h away from the wall, which corresponds to the second grid point off the wall, i.e., $h \approx 2\Delta$. The other six components of the stencil are located Δ away from $\boldsymbol{x}^{\boldsymbol{0}}$ and are denoted as $\boldsymbol{x}^{\pm \boldsymbol{e}_i} = \boldsymbol{x}^{\boldsymbol{0}} \pm \Delta \boldsymbol{e}_i$ for $i = 1, 2, 3$, where $\boldsymbol{e}_i$ is a unit vector. The vector $\boldsymbol{e}_2$ is parallel to the wall-normal direction and $\boldsymbol{e}_1$ and $\boldsymbol{e}_3$ are oriented to form an orthogonal basis. The velocity components at the stencil points are denoted by $u_i^{\boldsymbol{0}}$ and $u_i^{\pm \boldsymbol{e}_i}$. The input variables are arranged as velocity differences

$$\tilde{u}_i^{\boldsymbol{0}} = u_i^{\boldsymbol{0}} - u_{i,\mathrm{wall}}, \tag{4.1a}$$

$$\tilde{S}_{ij} = (\delta_i u_j + \delta_j u_i)/2, \tag{4.1b}$$

$$\tilde{\Omega}_{ij} = (\delta_i u_j - \delta_j u_i)/2, \tag{4.1c}$$

where $\delta_i u_j = (u_j^{\boldsymbol{e}_i} - u_j^{-\boldsymbol{e}_i})/(2\Delta)$ and $u_{i,\mathrm{wall}}$ is the velocity at the wall. The velocities u_i are obtained by interpolation of the LES velocities to $\boldsymbol{x}^{\boldsymbol{0}}$ and $\boldsymbol{x}^{\pm \boldsymbol{e}_i}$.

The multi-space structure of a seven-point stencil offers important advantages over the

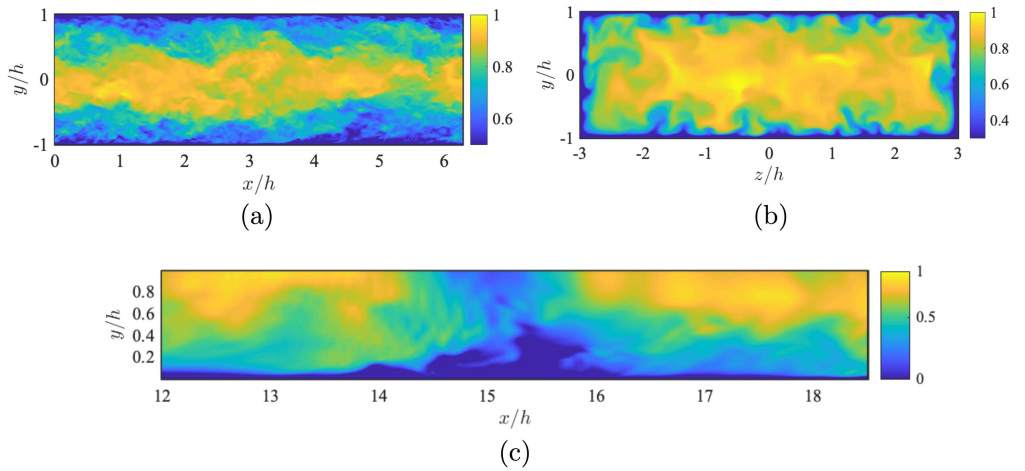

FIGURE 7. Three examples of the building block units taken as representative of the potential flow configurations. (a) Turbulent channel flow at $Re_\tau = 1000$, (b) turbulent duct at $Re_\tau = 180$ and aspect ratio 3, and (c) boundary layers with a separation bubble via blowing and suction at $Re_\tau \approx 180$. The colors are the instantaneous streamwise velocity normalized by the freestream/centerline velocity. Panels (a) and (c) show the velocity for a streamwise/wall-normal plane and panel (b) for a wall-normal/spanwise plane.

traditional single-point stencil. A key property is that it makes possible to discern among different types of flow, such as separation zones, mean-flow three-dimensionality, or even whether the input variable is within the boundary layer or the freestream. This capability is unavailable using single-point stencils. The flow-state variables $\tilde{u}_i^{\mathbf{0}}$, $\tilde{S}_{ij}$ and $\tilde{\Omega}_{ij}$ comply with Galilean invariance, as they are constructed using relative velocities. Note that δ_i differs from the discrete gradient operators in charLES and the stencil points do not necessarily coincide with the grid cell centers. In unstructured grids, the location of the cell centers could follow a complex pattern in space. Additionally, the discrete gradient operators may differ depending on the discretization method. Hence, the stencil selected aims at alleviating these problems by facilitating the model training process from DNS data and promoting generalizability for different numeric and grid strategies.

In addition to velocity information, the model also takes into account the grid size Δ, the distance to the wall h, the fluid properties ρ and ν, and the farfield velocity U_∞ (defined with respect to the wall velocity). To ease the classification of different flow regimes, we introduce a characteristic length-scale $\mathcal{L}$ and velocity scale $\mathcal{U}$ for each of the building blocks considered. In the turbulent channel, the characteristic scales are assumed to be the stress at the wall and the distance to the wall, which yield $\mathcal{L}_1 = h$ and $\mathcal{U}_1 = \sqrt{\tau_w/\rho}$ (Townsend 1976). In the steady turbulence with mean-flow three-dimensionality, such as flow in corners, the fluid motions are controlled by the momentum flux and mean-shear. Characteristic scales consistent with the previous argument are $\mathcal{U}_2 = \sqrt{\tau_w/\rho}$ and $\mathcal{L}_2 = \mathcal{U}_2/S$ (Lozano-Durán & Bae 2019), where $S = ||\nabla\langle\boldsymbol{u}\rangle||$. In separated flows, the mean momentum equation is balanced by the viscous terms and pressure gradient, which gives $\mathcal{U}_3 = [(\partial\langle p\rangle/\partial s)\nu/\rho]^{1/3}$ and $\mathcal{L}_3 = \nu/\mathcal{U}_3$ (Stratford 1959), where $\langle p\rangle$ is mean pressure and s the mean streamwise direction. The values of $\partial\langle p\rangle/\partial s$

and S are evaluated using the discrete seven-point stencil and the wall stress vector τ_w is obtained from the previous time step.

Finally, the input to the wall model comprises the non-dimensional groups formed by the dimensional set

$$\left\{\tilde{u}_i^{\mathbf{0}}, \tilde{S}_{ij}, \tilde{\Omega}_{ij}; \mathcal{U}_k, \mathcal{L}_k; U_\infty, \rho, \nu, \Delta, h: \ i,j,k = 1,2,3\right\}, \tag{4.2}$$

which constitutes a collection of local Reynolds numbers and velocity differences non-dimensionalized by the characteristic scales. Examples of non-dimensional input variables can be found in Figure 6.

The output variables are divided into two sets: the wall stress vector expressed as $10^3 \times \boldsymbol{\tau_w}/(\rho U_\infty^2)$ and the information about the model flow classification and confidence on the solution. The last two outputs are explained in more detail in the next subsection.

4.3. *Neural network architecture and training*

The predictor-classifier structure is outlined in Figure 6. The predictor is a deep feed-forward neural network with 4 hidden layers and 30 neurons per layer. Both the inputs and outputs of the predictor are standardized. The classifier is a Bayesian neural network with 3 hidden layers and 15 neurons per layer. The activation functions selected for the hidden layers are hyperbolic tangent sigmoid transfer functions and rectified linear activation transfer functions. The present layout was found to give a fair compromise between neural network complexity and predictive capabilities. Nonetheless, future versions of the model might be accompanied by a systematic optimization of the neural network architecture.

Note that we would not even need a neural network to perform the steps above. The classification step can be conducted by means of other clustering techniques (such as k-means analysis), and the wall-stress prediction might be attained by switching between different analytic models (akin to the equilibrium wall model in Eq. (2.1)) according to the flow classification. Nonetheless, neural networks have shown excellent performance in classification tasks, and they are a convenient tool to build non-linear interpolations among datasets.

The training is performed using the following DNS databases: turbulent channel flows at $Re_\tau \approx 350, 550, 1000, 2000$ and 4200 (Lozano-Durán & Jiménez 2014), turbulent ducts at $Re_\tau \approx 180$ and 390 and aspect ratios equal to 1, 3, 6 and 10 (Vinuesa *et al.* 2014), and turbulent boundary layers with a separation bubble via blowing and suction at $Re_\tau \approx 180$ following the setup from Na & Moin (1998). The input signal is obtained by sampling the DNS data for various fictitious (isotropic) grid resolutions ranging from $\Delta/\delta = 0.01$ to 1 and at multiple wall-normal locations from 0.01δ to δ, where δ is the boundary-layer thickness (or channel half-height). The DNS velocity is averaged within a sphere of radius Δ centered at the location of $\boldsymbol{x}^{\mathbf{0}}$ (similarly for $\boldsymbol{x}^{\pm \boldsymbol{e}_i}$). The output is taken as the wall stress averaged over the surface area Δ^2. The training set is also augmented by performing arbitrary rotations of the frame of reference. The neural network is trained using Bayesian regularization backpropagation by randomly dividing the training date into two groups, the training set (80% of the data) and test set (20% of the data).

5. Model validation: Results of WMLES with SCMv1

We validate the model in the NASA Juncture Flow Experiment. The problem setup is identical to the one described in Section 2 replacing the equilibrium wall model by

		Location (a)	Location (b)	Location (c)
Classification	Flat plate flow	91%	27%	20%
	Corner flow	9%	73%	52%
	Separated flow	0%	0%	28%
Confidence		96%	92%	20%
Error SCMv1		1.4%	7.4%	78.9%
Error EQWM		2.0%	24.5%	98.7%

TABLE 1. The flow classification, confidence on the solution, and error in the mean velocity profiles by SCMv1. The errors in the last row are for WMLES with EQWM. The locations are (a) upstream region of the fuselage, (b) wing-body juncture, and (c) wing-body juncture close to the trailing edge.

the SCMv1. The prediction of the mean velocity profiles is presented in Figure 8 and compared with WMLES with EQWM for the three locations under consideration. Table 1 contains information about the flow classification and confidence on the solution at each location. The relative error on the prediction, quantified as $||\boldsymbol{u}^{\rm exp}-\boldsymbol{u}||/||\boldsymbol{u}^{\rm exp}||$, is included in the last rows of Table 1 for both SCMv1 and EQWM.

Figure 8(a) shows that the predictions for SCMv1 and EQWM at the fuselage location are roughly identical. In both cases, the wall stress is within 2% accuracy as reported in previous investigations (Lozano-Durán *et al.* 2020). The flow is identified by SCMv1 as a flat-plate turbulence with 96% confidence. The outcome is expected as SCMv1 was trained in turbulent channel flows and we have argued that the boundary layer at the fuselage resembles a ZPGTBL. The most notable improvement is found at the juncture location (Figure 8b): SCMv1 provides an augmented value of the wall stress, which alleviates the overprediction of u and w using EQWM. The new wall-stress prediction of the mean velocity profiles is to within 7.4% error, compared with the 24.5% error using EQWM. The flow is classified as predominantly corner flow with some traces of flat-plate turbulence. The confidence in the prediction is also above 90%.

Finally, the performance of SCMv1 in the separated region (Figure 8c) is the poorest of all three locations, but also the most interesting. There is a moderate improvement on the mean velocity prediction by SCMv1 with respect to EQWM, but this is still far from being satisfactory and errors remain above 78.9%. Interestingly, SCMv1 classifies the flow as a mix of flat plate turbulence, corner flow, and separated flow. Moreover, despite the erroneous prediction by SCMv1, the model prompts a warning about its poor performance, which is evidenced by the low confidence on the wall-stress prediction ($\sim$20%). The deficient performance of both wall models is not surprising if we note that the separation zone has a wall-normal thickness of 0.3δ, whereas the WMLES grid size is $\Delta \approx 0.2\delta$. Thus, there is only one grid point across the separation bubble. Despite the fact that the model was trained in separated flows, numerical errors and SGS model errors dominate the LES solution in this case. These errors hinder the capability of SCMv1 to classify the flow. Nonetheless, the ability of SCMv1 to assess the confidence on the prediction is a competitive advantage with respect to traditional wall models.

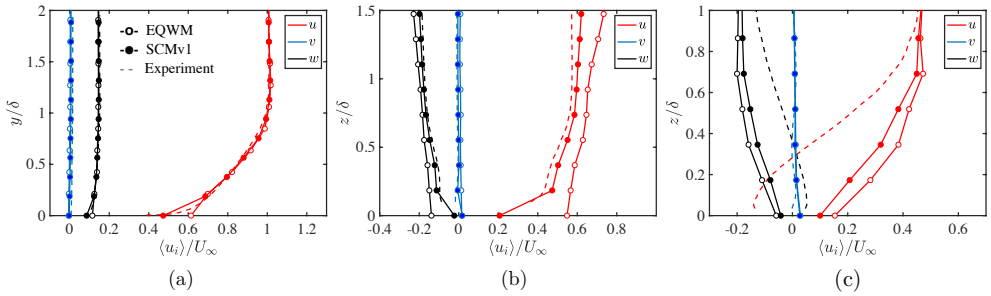

FIGURE 8. The mean velocity profiles at (a) upstream region of the fuselage at $x = 1168.4$ mm and $z = 0$ mm, (b) wing-body juncture at $x = 2747.6$ mm and $y = 239.1$ mm, and (c) wing-body juncture close to the trailing edge at $x = 2922.6$ mm and $y = 239.1$ mm. Solid lines with open symbols are for WMLES with EQWM and closed symbols for WMLES with SCMv1. Dashed lines are experiments. Colors denote different velocity components. The distances y and z are normalized by the local boundary-layer thickness δ at each location.

6. Conclusions and outlook

The prediction of aircraft aerodynamic quantities of interest remains among the most pressing challenges for computational fluid dynamics, and it has been highlighted as a Critical Flow Phenomena in the NASA CFD Vision 2030 (Slotnick *et al.* 2014). The aircraft aerodynamics are inherently turbulent with mean-flow three-dimensionality, often accompanied by laminar-to-turbulent transition, flow separation, secondary flow motions at corners, and shock wave formation, to name a few. However, the most widespread wall models are built upon the assumption of statistically-in-equilibrium wall-bounded turbulence and do not faithfully account for the wide variety of flow conditions described above. This raises the question of how to devise models capable of accounting for such a vast and rich collection of flow physics in a feasible manner.

In this preliminary work, we have proposed tackling the wall-modeling challenge by devising the flow as a collection of building blocks, whose information enables the prediction of the stress as the wall. We refer to the wall model as SCMv1 (self-critical model version 0.1). The model relies on the assumption that simple canonical flows (such as turbulent channel flows, boundary layers, pipes, ducts, speed bumps, etc) contain the essential flow physics to devise accurate models. Three types of building block units were used to train the model, namely, turbulent channel flows, turbulent ducts and turbulent boundary layers with separation. This limited training set will be extended in future versions of the model. The approach is implemented using two interconnected artificial neural networks: a classifier, which identifies the contribution of each building block in the flow; and a predictor, which estimates the wall stress via non-linear combinations of building-block units. The output of the model is accompanied by the confidence in the prediction. The latter value aids the detection of areas where the model underperforms, such as flow regions that are not representative of the building blocks used to train the model. This is the self-critical component of the SCM and is considered a key step for developing reliable models. For example, the present model will provide a low confidence value in the presence of a flow that it has never seen before (e.g., a shock wave), or when the input velocity is outside of the boundary layer.

The model was validated in a unseen case representative of external aerodynamic applications: the NASA Juncture Flow Experiment. The case is a generic full-span wing-fuselage body at Reynolds number $Re = 2.4 \times 10^6$. We have characterized the WMLES errors in the prediction of mean velocity profiles with SCMv1 and a widely used equilibrium wall model. Three different locations over the aircraft have been considered: the upstream region of the fuselage, the wing-body juncture, and the wing-body juncture close to the trailing edge. The last two locations are characterized by strong mean-flow three-dimensionality and separation. We have shown that SCMv1 outperforms the EQWM in the three locations investigated. However, the most remarkable result is not the higher accuracy of SCM which, due to the larger number of degrees of freedom in the model, is deemed to outperform the EQWM. Instead, we remark on (1) the success of the model in providing confidence levels in the wall-stress prediction and (2) its potential to account for new flow physics by including additional building block units. The promising performance of SCMv1 presented here is still limited to a few observations and thus should be taken with caution. Further investigation is needed to systematically characterize errors at multiple grid resolutions and flow configurations.

Several outstanding issues remain to be solved, such as the identification of meaningful building-block flows, the minimum number of blocks required to make accurate predictions, and their characteristic scales. The choice of input and output variables and their non-dimensionalization is also of paramount importance in obtaining a successful model. Here, we have used instantaneous data as input information but time-varying signals are probably needed to predict strongly unsteady effects. Another outstanding issue is the necessity of high-quality wind-tunnel experiments as a proxy for evaluating the accuracy of WMLES in real-world external aerodynamic applications. Useful measurements include pointwise time-averaged velocities and Reynolds stress profiles along with surface pressure and friction coefficients. The scarcity to date of granular experimental quantities hinders our ability to assess and improve the performance of WMLES in more realistic scenarios.

We have argued that truly revolutionary improvements in WMLES will encompass advancements in numerics, grid generation, and wall/SGS modeling. Here, we have focused on wall-modeling and much work remains to be done on other fronts. There is obviously a data science component to the problem too, such as the need for efficient and reliable machine-learning techniques for data classification and regression. However, the main emphasis of this work has been on the physical understanding of the problem rather than on the details of neural network architecture at hand. The comment in the introduction about the shallowness of the statement "LES modeling will be solved by machine learning" is just a reminder that problems are not solved by tools but by people.

Acknowledgments

A.L.-D. acknowledges the support of NASA under grant No. NNX15AU93A.

REFERENCES

Bae, H. J., Lozano-Durán, A., Bose, S. T. & Moin, P. 2019 Dynamic slip wall model for large-eddy simulation. *J. Fluid Mech.* **859**, 400–432.

Balaras, E., Benocci, C. & Piomelli, U. 1996 Two-layer approximate boundary conditions for large-eddy simulations. *AIAA J.* **34**, 1111–1119.

Bermejo-Moreno, I., Campo, L., Larsson, J., Bodart, J., Helmer, D. & Eaton, J. K. 2014 Confinement effects in shock wave/turbulent boundary layer interactions through wall-modelled large-eddy simulations. *J. Fluid Mech.* **768**, 5–62.

Bodart, J. & Larsson, J. 2011 Wall-modeled large eddy simulation in complex geometries with application to high-lift devices. *Center for Turbulence Research - Annual Research Briefs* pp. 37–48.

Bose, S. T. & Moin, P. 2014 A dynamic slip boundary condition for wall-modeled large-eddy simulation. *Phys. Fluids* **26**, 015104.

Bose, S. T. & Park, G. I. 2018 Wall-modeled large-eddy simulation for complex turbulent flows. *Annu. Rev. Fluid Mech.* **50**, 535–561.

Brunton, S. L., Noack, B. R. & Koumoutsakos, P. 2020 Machine learning for fluid mechanics. *Ann. Rev. Fluid Mech.* **52**, 477–508.

Cabot, W. H. & Moin, P. 2000 Approximate wall boundary conditions in the large-eddy simulation of high Reynolds number flow. *Flow Turbul. Combust.* **63**, 269–291.

Choi, H. & Moin, P. 2012 Grid-point requirements for large eddy simulation: Chapman's estimates revisited. *Phys. Fluids* **24**, 011702.

Chung, D. & Pullin, D. I. 2009 Large-eddy simulation and wall modelling of turbulent channel flow. *J. Fluid Mech.* **631**, 281–309.

Deardorff, J. 1970 A numerical study of three-dimensional turbulent channel flow at large Reynolds numbers. *J. Fluid Mech.* **41**, 453–480.

Duraisamy, K., Iaccarino, G. & Xiao, H. 2019 Turbulence modeling in the age of data. *Ann. Rev. Fluid Mech.* **51**, 357–377.

Fukami, K., Fukagata, K. & Taira, K. 2019 Super-resolution reconstruction of turbulent flows with machine learning. *J. Fluid Mech.* **870**, 106–120.

Gamahara, M. & Hattori, Y. 2017 Searching for turbulence models by artificial neural network. *Phys. Rev. Fluids* **2**, 054604.

Germano, M., Piomelli, U., Moin, P. & Cabot, W. H. 1991 A dynamic subgrid-scale eddy viscosity model. *Phys. Fluids* **3**, 1760.

Hickel, S., Franz, S., Adams, N. A. & Koumoutsakos, P. 2004 Optimization of an implicit subgrid-scale model for LES. In *Proc. 21st Int. Congr. Theoret. Appl. Mech., Warsaw, Poland*.

Kawai, S. & Larsson, J. 2012 Wall-modeling in large eddy simulation: Length scales, grid resolution, and accuracy. *Phys. Fluids* **24**, 015105.

Kawai, S. & Larsson, J. 2013 Dynamic non-equilibrium wall-modeling for large eddy simulation at high reynolds numbers. *Phys. Fluids* **25**, 015105.

Kegerise, M. A., Neuhart, D., Hannon, J. & Rumsey, C. L. 2019 An experimental investigation of a wing-fuselage junction model in the NASA Langley 14- by 22-foot Subsonic Wind Tunnel. *AIAA Paper* 2019-0077.

Larsson, J., Kawai, S., Bodart, J. & Bermejo-Moreno, I. 2016 Large eddy simulation with modeled wall-stress: recent progress and future directions. *Mech. Eng. Rev.* **3**, 1–23.

Lilly, D. K. 1992 A proposed modification of the Germano subgrid-scale closure method. *Phys. Fluids* **4**, 633–635.

Lozano-Durán, A. & Bae, H. 2019 Characteristic scales of Townsend's wall-attached eddies. *J. Fluid Mech.* **868**, 698–725.

Lozano-Durán, A., Bose, S. T. & Moin, P. 2020 Performance of wall-modeled

LES for external aerodynamics in the NASA juncture flow. *Annual Research Briefs*, Center for Turbulence Research, Stanford University, pp. 33–48.

Lozano-Durán, A. & Jiménez, J. 2014 Effect of the computational domain on direct simulations of turbulent channels up to $Re_\tau = 4200$. *Phys. Fluids* **26**, 011702.

Maulik, R. & San, O. 2017 A neural network approach for the blind deconvolution of turbulent flows. *J. Fluid Mech.* **831**, 151–181.

Na, Y. & Moin, P. 1998 Direct numerical simulation of a separated turbulent boundary layer. *J. Fluid Mech.* **374**, 379–405.

Park, G. I. & Moin, P. 2014 An improved dynamic non-equilibrium wall-model for large eddy simulation. *Phys. Fluids* **26**, 015108.

Piomelli, U. & Balaras, E. 2002 Wall-layer models for large-eddy simulations. *Annu. Rev. Fluid Mech.* **26**, 349–374.

Piomelli, U., Ferziger, J., Moin, P. & Kim, J. 1989 New approximate boundary conditions for large eddy simulations of wall-bounded flows. *Phys. Fluids* **1**, 1061–1068.

Rumsey, C. L., Carlson, J. & Ahmad, N. 2019 FUN3D juncture flow computations compared with experimental data. *AIAA Paper* 2019-0079.

Sarghini, F., De Felice, G. & Santini, S. 2003 Neural networks based subgrid scale modeling in large eddy simulations. *Comput. Fluids* **32**, 97–108.

Schumann, U. 1975 Subgrid scale model for finite difference simulations of turbulent flows in plane channels and annuli. *J. Comp. Phys.* **18**, 376–404.

Slotnick, J., Khodadoust, A., Alonso, J., Darmofal, D., Gropp, W., Lurie, E. & Mavriplis, D. 2014 *CFD Vision 2030 Study: A Path to Revolutionary Computational Aerosciences*.

Spalart, P. R. 2009 Detached-eddy simulation. *Annu. Rev. Fluid Mech.* **41**, 181–202.

Stratford, B. S. 1959 The prediction of separation of the turbulent boundary layer. *J. Fluid Mech.* **5**, 1–16.

Townsend, A. A. 1976 *The structure of turbulent shear flow*. Cambridge Univ Press.

Vinuesa, R., Noorani, A., Lozano-Durán, A., Khoury, G. K. E., Schlatter, P., Fischer, P. F. & Nagib, H. M. 2014 Aspect ratio effects in turbulent duct flows studied through direct numerical simulation. *J. Turbul.* **15**, 677–706.

Vollant, A., Balarac, G. & Corre, C. 2017 Subgrid-scale scalar flux modelling based on optimal estimation theory and machine-learning procedures. *J. Turbul.* **18**, 854–878.

Wang, M. & Moin, P. 2002 Dynamic wall modeling for large-eddy simulation of complex turbulent flows. *Phys. Fluids* **14**, 2043–2051.

Xie, C., Wang, J., Li, H., Wan, M. & Chen, S. 2019 Artificial neural network mixed model for large eddy simulation of compressible isotropic turbulence. *Phys. Fluids* **31**, 085112.

Yang, X. I. A., Sadique, J., Mittal, R. & Meneveau, C. 2015 Integral wall model for large eddy simulations of wall-bounded turbulent flows. *Phys. Fluids* **27**, 025112.

Yang, X. I. A., Zafar, S., Wang, J.-X. & Xiao, H. 2019 Predictive large-eddy-simulation wall modeling via physics-informed neural networks. *Phys. Rev. Fluids* **4**, 034602.